Supporting Information

Descriptors of Oxygen-Evolution Activity for Oxides: A Statistical Evaluation

Wesley T. Hong[1,*], Roy E. Welsch[2], Yang Shao-Horn[1,3]

[1] *Department of Materials Science & Engineering,*

[2] *Sloan School of Management,*

[3] *Department of Mechanical Engineering, Massachusetts Institute of Technology, Cambridge, MA 02139, USA*

Corresponding Authors

* (W.T.H.) E-mail: whong@mit.edu. Phone: +1 (617) 324-3718.

* (Y.S.-H.) E-mail: shaohorn@mit.edu. Phone: +1 (617) 253-2259.

Index	**Page**

Additional discussion on data preparation

Aggregation and standardization of descriptors

Descriptor values were obtained as described in the main text. Experimental structural values were obtained from literature.[1-34]

All descriptor values were standardized prior to training the models to correct for differences in their scale. This means that each descriptor (x) was expressed in units of standard deviations using the following transformation:

$$x' = \frac{x - \bar{x}}{s_x}$$

where $\bar{x}$ is the mean value of the descriptor for all oxides in the data set, and s_x is the standard deviation. The descriptor values under this transformation represent how different an oxide's value is compared to the rest of the data set. The test data descriptor values were standardized using the means and standard deviations from the training set in order to replicate the process of applying the model to new data.

Standardization of OER activity

Here we discuss the behavior of the data during the standardization process in more detail. The relative change for a single material across studies is approximately equal when stratified by the parameter being fixed (i.e. overpotential or log-current-density), as evident from the distribution of the most frequent material studied other than $LaCoO_3$ – $La_{0.6}Sr_{0.4}CoO_3$ (**Table S1a**). However, the range of relative changes in log-current-density can be very different from those in overpotential (**Fig. S1**). Because the spread of compounds measured using overpotential and current density should be similar (the most active and least active compounds are identical for both the overpotential and current data sets), one approach to standardize the relative changes in overpotentials and current-densities is to normalize by their respective standard deviations.

The resulting distribution is shown in **Fig. S2**, illustrating similar distributions of overpotential and current-density measurements. This process is equivalent to standardization under the assumption that the population mean relative change vs. $LaCoO_3$ is 0. It can be shown that this hypothesis cannot be rejected by the data (**Fig. S3**).

Table S1. Distribution of $La_{0.6}Sr_{0.4}CoO_3$ OER activity metrics after scaling as the change relative to the OER activity of $LaCoO_3$ reported within the study. Note the similarity in values for measurements that fix the same parameter (±15%).

Reference	OER activity metric	Relative change vs. $LaCoO_3$
Matsumoto et al.[35]	η @ 40 mA/cm^2	0.1334
Matsumoto et al.[35]	η @ 60 mA/cm^2	0.1595
Jain et al.[36]	η @ 10 mA/cm^2	0.1848
Jain et al.[36]	η @ 100 mA/cm^2	0.1752
Bockris, Otagawa[37]	i @ 1.53 V vs. RHE	0.2847
This work	i @ 1.60 V vs. RHE	0.2949

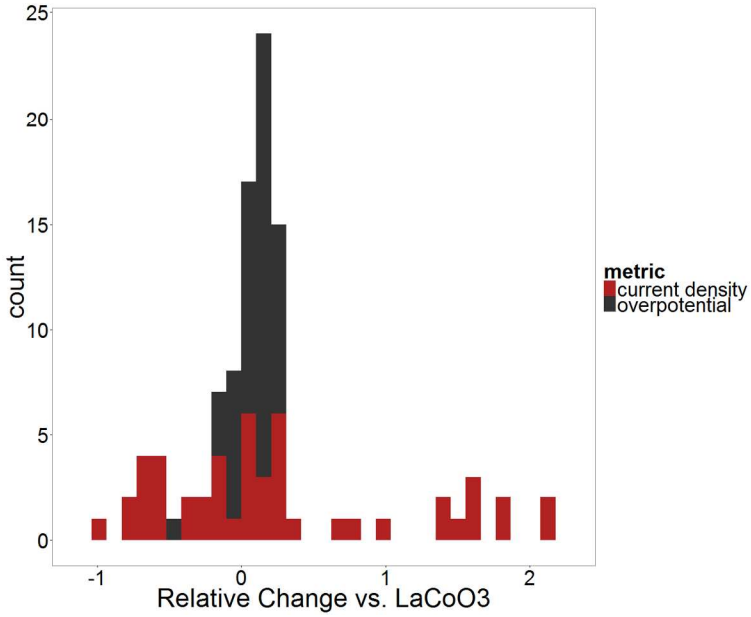

Figure S1. Histogram of the OER activity distribution after converting all activity metrics to relative changes relative to the study's measurement on $LaCoO_3$. Note that the distribution density is localized near 0 for studies regardless of the activity metric, yet their spreads differ.

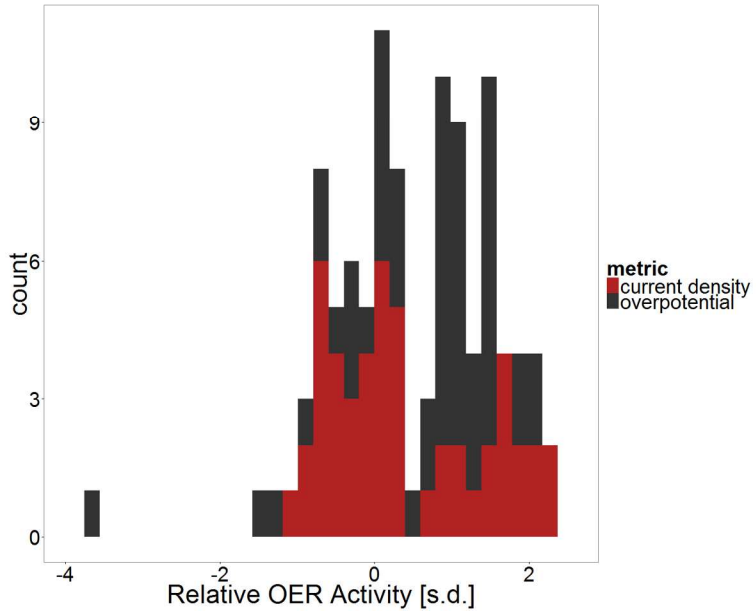

Figure S2. Histogram of the Relative OER Activity distribution, which takes the stratified distributions from Figure S1 and normalizes by their respective standard deviations. Note that the distributions are much more comparable after standardization.

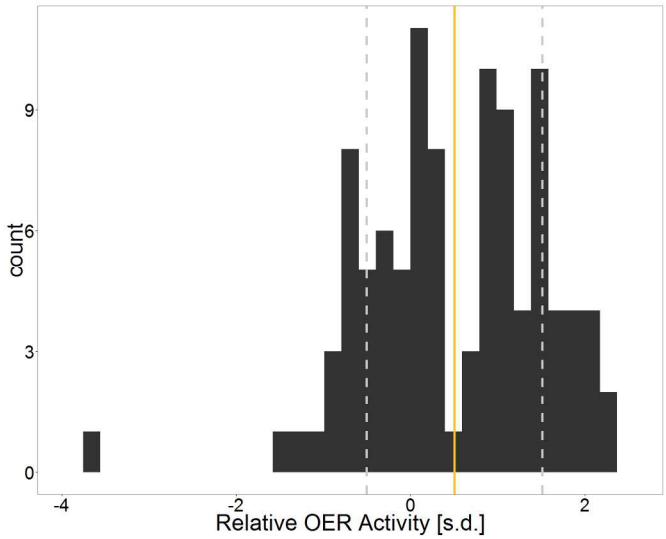

Figure S3. Histogram of the Relative OER Activity. Gold line indicates the distribution mean and dashed lines indicate one standard deviation. Under the null hypothesis that the perovskite population's mean relative change from $LaCoO_3$ is normally distributed and centered at 0, this sampling distribution is likely to occur, and the null hypothesis cannot be rejected. The apparent bimodality shows no apparent relationship with different studies and is likely due to sampling choices (Fig. S4).

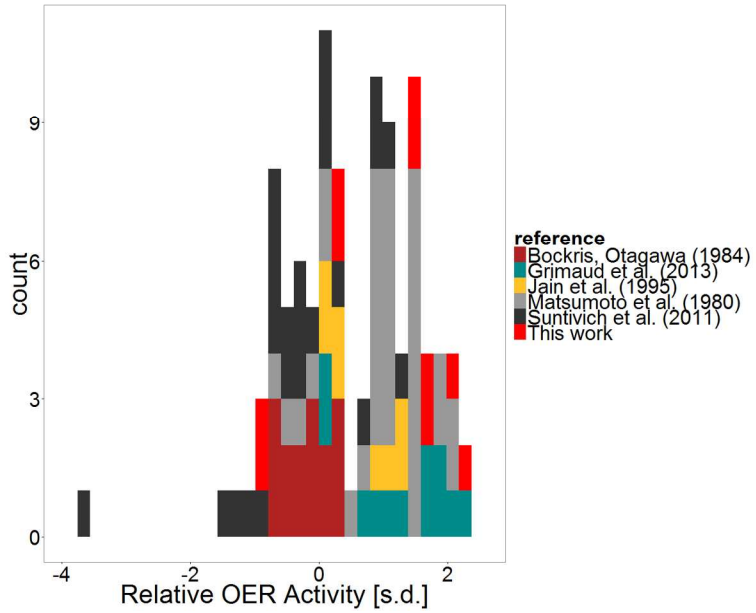

Figure S4. Histogram of the Relative OER Activity for different references. The apparent bimodality of the overall distribution shows no apparent relationship with the reference the data was taken from. Each study spans a fairly wide range of Relative OER Activities, also indicating that differences among studies are primarily due to the choice of catalysts studied.

Table S2. Distribution of $La_{0.6}Sr_{0.4}CoO_3$ Relative OER Activity, the standardized relative change in OER activity vs. $LaCoO_3$. Note that the standardization still has distinct values for OER activities quantified using different variables. The standard error is 0.44 s.d. in this case, which is a rough estimate of the standardization error across studies.

Reference	OER activity metric	Relative OER Activity [s.d.]
Matsumoto et al.[35]	η @ 40 mA/cm^2	0.9278
Matsumoto et al.[35]	η @ 60 mA/cm^2	1.1089
Jain et al.[36]	η @ 10 mA/cm^2	1.2845
Jain et al.[36]	η @ 100 mA/cm^2	1.2183
Bockris, Otagawa[37]	i @ 1.53 V vs. RHE	0.3156
This work	i @ 1.60 V vs. RHE	0.3270

Additional discussion on regression models and analysis protocol

Ordinary least squares (OLS) minimizes the sum of square errors between the model prediction and the experimental data during training. The solutions to OLS models are straightforward to compute, and p-values can be calculated assuming homoscedastic, normally distributed errors. In multiple OLS, the p-values of predictors can provide a clear indication of whether a variable has a statistically significant influence on the relative OER activity.

Rather than using a model with a user-defined number of predictors, several algorithms have been developed for selecting a subset of predictor variables (a process known as feature selection). In *forward selection*, an OLS model is initialized with no predictor variables. On each iteration, the predictor that improves the model the most is added. The final model is determined when adding a variable no longer leads to an improvement. *Backward elimination* operates in a similar iterative fashion but begins with all potential features, and removes one on each iteration. In our study, we used the Akaike information criterion[38] to measure the level of improvement when adding a variable.

Penalized regression methods depart from the least squares approach in OLS. Rather than minimizing the sum of square errors, a penalty function is added to constrain the optimization. This is particularly useful in problems with high dimensionality and multicollinearity. The family of L-norm penalty functions are typically used, and the new minimization can be written as:

$$L(\alpha, \lambda, \boldsymbol{\beta}) = |\mathbf{y} - \mathbf{X}\boldsymbol{\beta}|^2 + (1-\alpha)\lambda \sum_{j=1}^{p} \left|\beta_j\right|^2 + \alpha\lambda \sum_{j=1}^{p} \left|\beta_j\right|$$

The first term is simply the sum of square errors, the second is a penalty that scales with the Euclidean distance (L2 penalty), and the third with absolute distance (L1 penalty).[38] The penalty

terms place a constraint on the size of the coefficients (often referred to as shrinkage). When the L2 penalty is given 100% weighting, this is referred to as *ridge regression*. In ridge regression, weakly important coefficients do not shrink completely to 0. In contrast, when the L1 penalty is included coefficients can shrink to 0. There are two primary algorithms for computing the solution with 100% L1 penalty weighting: *least angle regression (LAR)* and *LASSO*. Intermediate weightings can also be used, which are then referred to as *elastic nets*. In this study, we make use of ridge, LAR, LASSO, and three variants of elastic nets (25%, 50%, and 75% weightings referred to as EN1, EN2, and EN3, respectively). Because of the high dimensionality and multicollinearity of the problem, an aggressive approach to sample shrinkage was employed to reduce the number of important factors to consider in materials design: complexity parameters (λ for elastic nets and k for LAR) were chosen to have the highest complexity with CV error within one standard error of the minimum CV error.

Latent variable regression is another method that can mitigate multicollinearity and offers feature selection. Latent variable models relate the set of predictors to a set of latent variables that are used for regression. There are various methods for generating latent variables; in this study, we implement factor regression, which uses the joint variations in predictors to generate hidden factors revealing the relationship among predictors.[39] Factor loadings were fit using a linear regression model, requiring that factor scores be uncorrelated and of unit variance, and that the errors be independent.

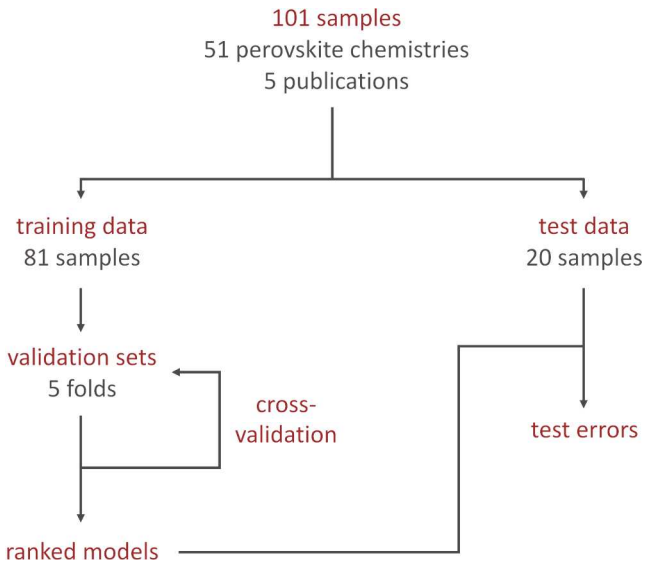

Figure S5. Flowchart of the data training, validation, and testing.

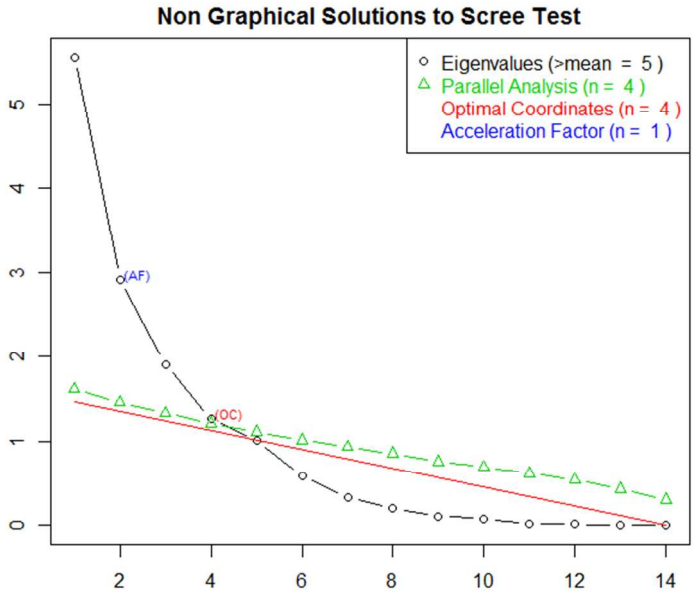

Figure S6. Plot of latent variable eigenvalues vs. the number of eigenvalues, obtained by factor analysis. Lines indicate the optimal number of latent variables to use for factor analysis based on different criteria. In this study, we used the Kaiser criterion, which states that the optimal number of latent variables considers only those with eigenvalues greater than 1.0, i.e. 5 latent variables (black line). Four latent variables could not be optimized by the package used (R CRAN stats[40]).

Additional discussion on regression results

Penalized regression models

Models that implement some level of the L1 penalty (elastic nets, LASSO, LAR) are fairly comparable and have the lowest CV errors when compared to solely using the L2 penalty (ridge) or the factor analysis latent variables, although the differences are minor. The descriptors with wider ranges in $|\beta|$ (**Fig. 5**) illustrate that multicollinearity effects still influence the results to some degree, however, their sporadic inflationary effects are more controlled using these penalized regression models. Of particular note are the ranges associated with d electrons, charge-transfer energy, M–O–M bond angle, and M–M distance, M–O bond length, and magnetic moment. As evident from the pairwise correlations (**Fig. S7**), inverse collinearity between the charge-transfer energy and M–O–M bond angle can result in increases in one coefficient at the expense of the other. A similar effect can occur between d electrons and magnetic moment as well as M–M distance and M–O bond length.

Factor regression

Under the assumption of normally distributed, homoscedastic errors, no significant difference between the coefficients of electron occupancy and covalency on the relative OER activity was observed. A two-sample Z-test under the null hypothesis that the mean coefficient values are identical yields a score of 2.3 ($p = 0.020$ for a two-sided test). This is equivalent to $p = 0.080$ after applying the Bonferroni family-wise error correction for four hypothesis tests on pairs with similar coefficients (i.e. electron occupancy/covalency, structure/exchange interaction, structure/ electrostatic, and exchange interaction/electrostatic). A similar p-value ($p = 0.081$) is obtained when controlling the false discovery rate.[41] We thus conclude that it cannot be discerned whether electron occupancy or covalency has a stronger influence on the relative OER activity.

OER descriptor correlation matrix

Fig. S7 illustrates the distributions and collinearity among the studied descriptors through the pairwise correlation coefficients (*r*). The descriptor distributions, shown along the diagonal, are non-uniform and do not show many outliers. The correlation matrix highlights relationship clusters of different descriptors seen in the factor analysis. For instance, descriptors that are dependent on the number of electrons occupying specific transition metal states, such as the number of d electrons, e_g occupancy, and the magnetic moment, show correlations among each other. Different parameters characterizing the relative energy of electrons also appear related, including the oxidation state, Madelung site potentials (M and O), ionization energy, Hubbard U, and the charge-transfer energy. Likewise, structural descriptors describing atomic positions and the geometry of bonds are correlated, e.g. the optimality of the tolerance factor from ideality, average M–O bond length, average M–O–M bond angle, and average M–M distance. This coupling convolutes the physical underpinning of QSARs using single descriptors, emphasizing the need for more robust analysis to optimally select descriptors. An interesting observation is that descriptors from any one group generally do not show strong correlations with those of other groups; for instance, the tolerance factor does not correlate with any electron occupancy or electron energy descriptors.

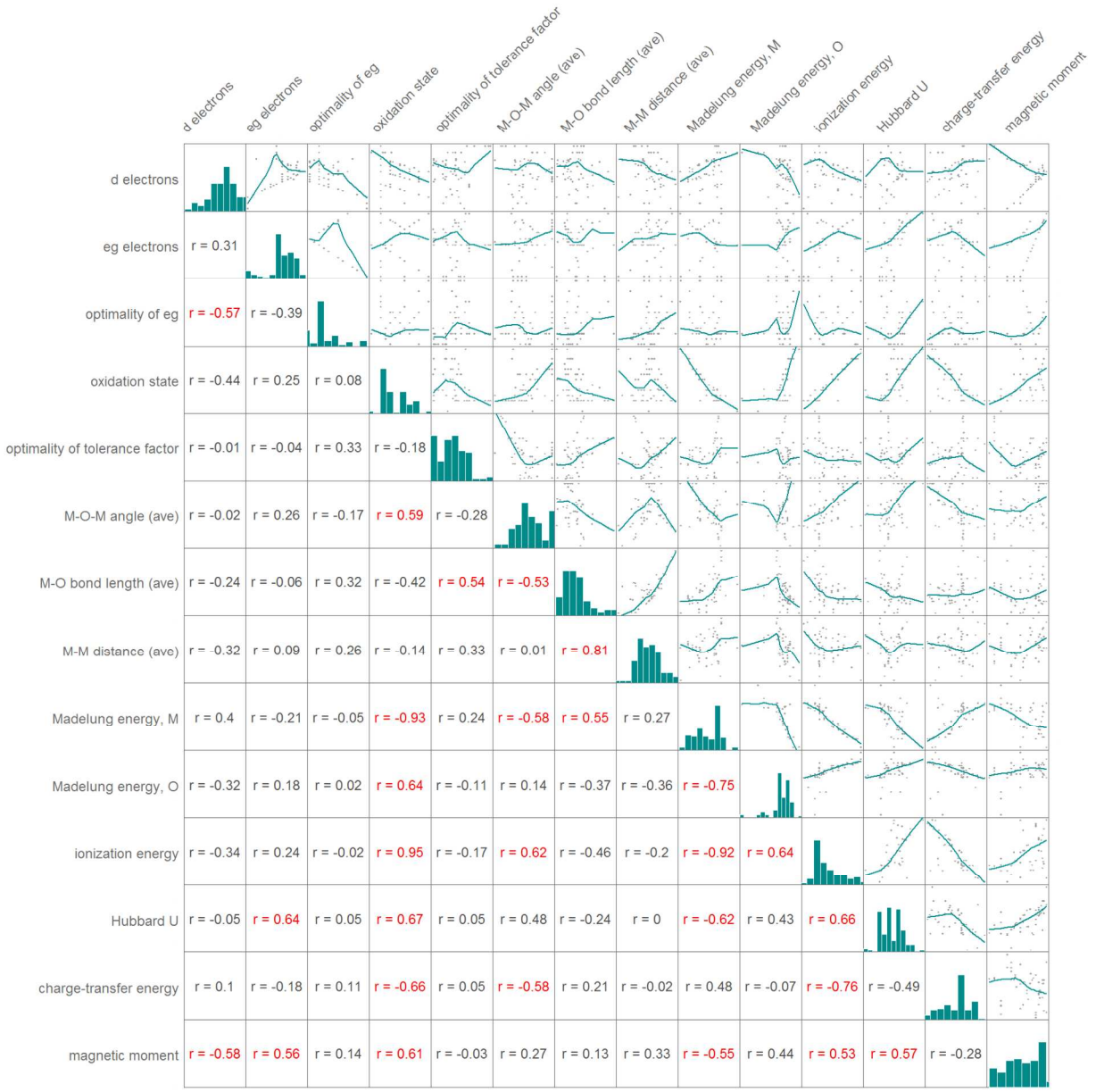

Figure S7. Correlation matrix for the 14 descriptors studied. The diagonal illustrates histograms of the descriptor value distributions. The upper half illustrates the pairwise scatterplots, with a LOESS smoothing curve shown in green. The lower half provides the corresponding Pearson correlation coefficients (r), with correlations larger than 0.5 emphasized in red. The magnitude of correlation coefficients expected from spurious correlations was estimated using 5000 non-parametrically bootstrapped samplings. Two-sided 95% confidence intervals of the correlation coefficients were consistently between $r = –0.2$ and 0.2, suggesting that the large correlation coefficients are real.

Table S3. Multiple linear regression using all 14 descriptors. Only one of the p-values is significant at the $\alpha = 0.004$ threshold (Bonferroni family-wise error correction for 14 hypothesis tests), marked (*). Corresponding variance inflation factors (VIF) are a measure of descriptor multicollinearity; a typical rule of thumb is VIF > 10 indicates high multicollinearity.

Descriptor	***β***	**Std Error**	***p*-value**	**VIF**
d electrons	–0.244	0.347	0.484	23.2
e_g electrons	0.638	0.316	0.048	24.8
optimality of e_g	–0.289	0.110	0.011	2.9
oxidation state	0.866	0.428	0.047	20.7
optimality of tolerance factor	0.293	0.100	0.004*	2.3
M – O – M bond angle (ave)	0.451	0.210	0.036	9.9
M – O bond length (ave)	–0.109	0.444	0.808	41.3
M – M distance (ave)	–0.379	0.287	0.192	19.7
Madelung potential, M	6.887	4.962	0.170	6708
Madelung potential, O	–2.095	1.686	0.218	865
ionization energy	11.056	8.801	0.213	21909
Hubbard *U*	0.041	0.137	0.766	5.3
charge-transfer energy	5.642	4.524	0.217	5252
magnetic moment	–0.779	0.330	0.021	27.4
CV error	0.544	0.147		
test error	0.468			

Table S4. Penalized regression results.

Descriptor	Ridge	Elastic Net 1	Elastic Net 2	Elastic Net 3	LASSO	LAR
d electrons	0.191	0.295	0.339	0.358	0.401	0.353
e_g electrons	0.092	0.008				
optimality of e_g	–0.164	–0.180	–0.142	–0.150	–0.156	–0.216
oxidation state	0.029					
optimality of tolerance factor	0.108	0.099	0.034	0.087	0.123	0.181
M – O – M bond angle (ave)	0.121	0.147	0.126	0.183	0.210	0.384
M – O bond length (ave)	–0.079	–0.054	–0.032	–0.001	0	0.233
M – M distance (ave)	–0.076	–0.054	–0.024	–0.074	–0.094	–0.310
Madelung potential, M	0.013					
Madelung potential, O	–0.033					
ionization energy	0.063					
Hubbard U	0.088	0.093	0.062	0.067	0.068	0.132
charge-transfer energy	–0.152	–0.217	–0.222	–0.248	–0.258	–0.229
magnetic moment	–0.109	–0.033				–0.071
complexity parameter	λ = 0.905	λ = 0.287	λ = 0.229	λ = 0.115	λ = 0.072	k = 9
CV error	0.515	0.513	0.538	0.538	0.501	0.484
CV error SE	0.054	0.051	0.092	0.063	0.053	0.035
test error	0.454	0.465	0.507	0.471	0.452	0.422

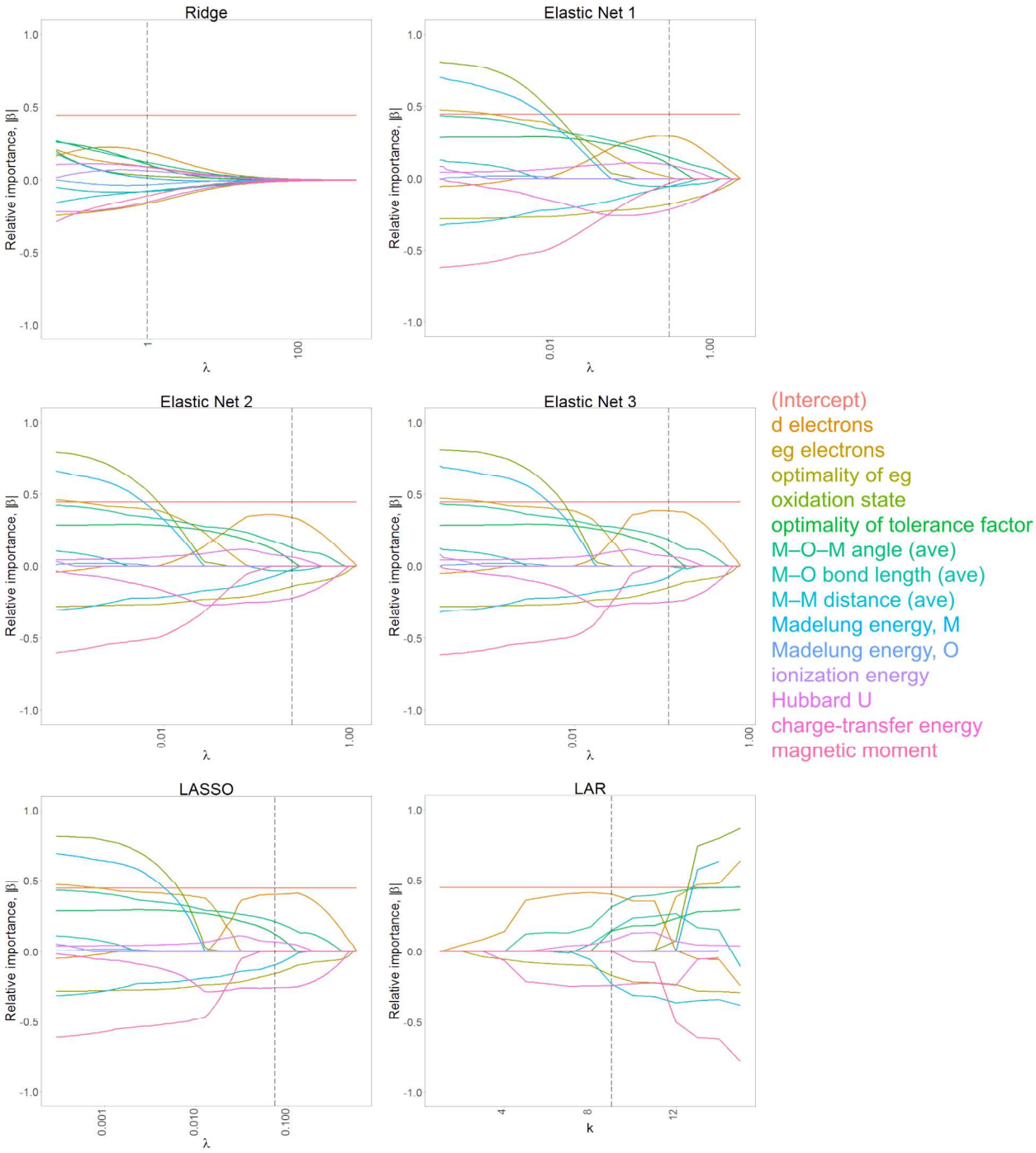

Figure S8. Relative importance of descriptors as a function of model's complexity parameter for the penalized regression models. Dashed lines illustrate complexity parameter value selected. Near the optimized point, changes in the relative importance of descriptors are small compared to the differences across models, indicating the relative importance is more sensitive to the cost function than the complexity parameter.

Supporting Information References

(1) Gallagher, P. K.; Johnson, J. D. W.; Vogel, E. M. Preparation, Structure, and Selected Catalytic Properties of the System $LaMn_{1-x}Cu_xO_{3-y}$. *J. Am. Ceram. Soc.* **1977**, *60*, 28-31.

(2) Devi, P. S.; Rao, M. S. Preparation, Structure, and Properties of Strontium-Doped Lanthanum Chromites: $La_{1-x}Sr_xCrO_3$. *J. Solid State Chem.* **1991**, *98*, 237-244.

(3) Komornicki, S.; Fournes, L.; Grenier, J. C.; Menil, F.; Pouchard, M.; Hagenmuller, P. Investigation of Mixed Valency Ferrites $La_{1-x}Ca_xFeO_{3-y}$ ($0 < x < 0.50$) with the Perovskite Structure. *Mater. Res. Bull.* **1981**, *16*, 967-973.

(4) Poeppelmeier, K. R.; Leonowicz, M. E.; Scanlon, J. C.; Longo, J. M.; Yelon, W. B. Structure Determination of $CaMnO_3$ and $CaMnO_{2.5}$ by X-ray and Neutron Methods. *J. Solid State Chem.* **1982**, *45*, 71-79.

(5) García-Muñoz, J. L.; Rodríguez-Carvajal, J.; Lacorre, P.; Torrance, J. B. Neutron-Diffraction Study of $RNiO_3$ (R=La,Pr,Nd,Sm): Electronically Induced Structural Changes Across the Metal-Insulator Transition. *Phys. Rev. B*. **1992**, *46*, 4414-4425.

(6) Ryu, K. H.; Roh, K. S.; Lee, S. J.; Yo, C. H. Studies of Nonstoichiometry and Magnetic Properties of the Perovskite $Gd_{1-x}SrCoO_{3-y}$ System. *J. Solid State Chem.* **1993**, *105*, 550-560.

(7) Dann, S. E.; Currie, D. B.; Weller, M. T.; Thomas, M. F.; Al-Rawwas, A. D. The Effect of Oxygen Stoichiometry on Phase Relations and Structure in the System $La_{1-x}Sr_xFeO_{3-\delta}$ ($0 < x < 1$, $0 < \delta < 0.5$). *J. Solid State Chem.* **1994**, *109*, 134-144.

(8) Van Roosmalen, J. A. M.; Cordfunke, E. H. P.; Helmholdt, R. B.; Zandbergen, H. W. The Defect Chemistry of $LaMnO_{3+\delta}$. 2. Structural Aspects of $LaMnO_{3+\delta}$. *J. Solid State Chem.* **1994**, *110*, 100-105.

(9) Mitchell, J. F.; Argyriou, D. N.; Potter, C. D.; Hinks, D. G.; Jorgensen, J. D.; Bader, S. D. Structural Phase Diagram of $La_{1-x}Sr_xMnO_{3+\delta}$: Relationship to Magnetic and Transport Properties. *Phys. Rev. B*. **1996**, *54*, 6172-6183.

(10) Sakai, N.; Fjellvag, H.; Hauback, B. C. Structural, Magnetic, and Thermal Properties of $La_{1-t}Ca_tCrO_{3-\delta}$. *J. Solid State Chem.* **1996**, *121*, 202-213.

(11) Sathe, V. G.; Pimpale, A. V.; Siruguri, V.; Paranjpe, S. K. Neutron Diffraction Studies of Perovskite-Type Compounds $La_{1-x}Sr_xCoO_3$ ($x = 0.1, 0.2, 0.3, 0.4, 0.5$). *J. Phys.: Condens. Matter*. **1996**, *8*, 3889-3896.

(12) Radaelli, P. G.; Cox, D. E.; Marezio, M.; Cheong, S. W. Charge, Orbital, and Magnetic Ordering in $La_{0.5}Ca_{0.5}MnO_3$. *Phys. Rev. B*. **1997**, *55*, 3015-3023.

(13) Seim, H.; Fjellvag, H.; Hauback, B. C. Non-Stoichiometric $LaVO_3$. II. Powder Neutron Diffraction Study of Crystal and Magnetic Structure for $La_{1-x}VO_3$, $0.00 < x < 0.10$. *Acta Chem. Scand.* **1998**, *52*, 1301-1306.

(14) Tezuka, K.; Hinatsu, Y.; Nakamura, A.; Inami, T.; Shimojo, Y.; Morii, Y. Magnetic and Neutron Diffraction Study on Perovskites $La_{1-x}Sr_xCrO_3$. *J. Solid State Chem.* **1998**, *141*, 404-410.

(15) Alonso, J. A.; Martinez-Lope, M. J.; Casais, M. T.; Aranda, M. A. G.; Fernandez-Diaz, M. T. Metal-Insulator Transitions, Structural and Microstructural Evolution of $RNiO_3$ (R = Sm, Eu, Gd, Dy, Ho, Y) Perovskites: Evidence for Room-Temperature Charge Disproportionation in Monoclinic $HoNiO_3$ and $YNiO_3$. *J. Am. Chem. Soc.* **1999**, *121*, 4754-4762.

(16) Alonso, J. A.; Martinez-Lope, M. J.; Casais, M. T.; Martinez, J. L.; Demazeau, G.; Largeteau, A.; Garcia-Munoz, J. L.; Munoz, A.; Fernandez-Diaz, M. T. High-Pressure Preparation, Crystal Structure, Magnetic Properties, and Phase Transitions in $GdNiO_3$ and $DyNiO_3$ Perovskites. *Chem. Mater.* **1999**, *11*, 2463-2469.

(17) Caciuffo, R.; Rinaldi, D.; Barucca, G.; Mira, J.; Rivas, J.; Senaris-Rodriguez, M. A.; Radaelli, P. G.; Fiorani, D.; Goodenough, J. B. Structural Details and Magnetic Order of $La_{1-x}Sr_xCoO_3$ ($x < 0.3$). *Phys. Rev. B*. **1999**, *59*, 1068-1078.

(18) van Doorn, R. H. E.; Burggraaf, A. J. Structural Aspects of the Ionic Conductivity of $La_{1-x}Sr_xCoO_{3-\delta}$. *Solid State Ionics*. **2000**, *128*, 65-78.

(19) Fauth, F.; Suard, E.; Caignaert, V.; Domenges, B.; Mirebeau, I.; Keller, L. Interplay of Structural, Magnetic and Transport Properties in the Layered Co-based Perovskite $LnBaCo_2O_5$ (Ln = Tb, Dy, Ho). *Eur. Phys. J. B*. **2001**, *21*, 163-174.

(20) Blasco, J.; Sanchez, M. C.; Perez-Cacho, J.; Garcia, J.; Subias, G.; Camp, J. Synthesis and Structural Study of $LaNi_{1-x}Mn_xO_{3+\delta}$. *J. Phys. Chem. Solids*. **2002**, *63*, 781-792.

(21) Frontera, C.; García-Muñoz, J. L.; Carrillo, A. E.; Ritter, C.; Martín y Marero, D.; Caneiro, A. Structural and Magnetic Study of $PrBaCo_2O_{5+\delta}$ (δ=0.75) cobaltite. *Phys. Rev. B*. **2004**, *70*, 184428.

(22) Frontera, C.; García-Muñoz, J. L.; Llobet, A.; Aranda, M. A. G. Selective Spin-State Switch and Metal-Insulator Transition in $GdBaCo_2O_{5.5}$. *Phys. Rev. B*. **2002**, *65*.

(23) Henry, P. F.; Weller, M. T.; Wilson, C. C. Variable Temperature Powder Neutron Diffraction Study of $SmNiO_3$ through its M-I Transition Using a Combination of Samarium and Nickel Isotopic Substitution. *Chem. Mater.* **2002**, *14*, 4104-4110.

(24) Pissas, M.; Kallias, G.; Hofmann, M.; Többens, D. M. Crystal and Magnetic Structure of the $La_{1-x}Ca_xMnO_3$ compound (x=0.8,0.85). *Phys. Rev. B*. **2002**, *65*.

(25) Radaelli, P. G.; Cheong, S. W. Structural Phenomena Associated with the Spin-State Transition in $LaCoO_3$. *Phys. Rev. B*. **2002**, *66*.

(26) Chmaissem, O.; Dabrowski, B.; Kolesnik, S.; Mais, J.; Jorgensen, J. D.; Short, S. Structural and Magnetic Phase Diagrams of $La_{1-x}Sr_xMnO_3$ and $Pr_{1-y}Sr_yMnO_3$. *Phys. Rev. B*. **2003**, *67*, 094431.

(27) Dabrowski, B.; Kolesnik, S.; Baszczuk, A.; Chmaissem, O.; Maxwell, T.; Mais, J. Structural, Transport, and Magnetic Properties of $RMnO_3$ Perovskites (R=La, Pr, Nd, Sm, Eu, Dy). *J. Solid State Chem.* **2005**, *178*, 629-637.

(28) Taguchi, H.; Masunaga, Y.; Hirota, K.; Yamaguchi, O. Synthesis of Perovskite-Type $(La_{1-x}Ca_x)FeO_3$ ($0 \leq x \leq 0.2$) at Low Temperature. *Mater. Res. Bull.* **2005**, *40*, 773-780.

(29) Le Toquin, R.; Paulus, W.; Cousson, A.; Prestipino, C.; Lamberti, C. Time-Resolved in Situ Studies of Oxygen Intercalation into $SrCoO_{2.5}$, Performed by Neutron Diffraction and X-ray Absorption Spectroscopy. *J. Am. Chem. Soc.* **2006**, *128*, 13161-13174.

(30) Takami, T.; Zhou, J. S.; Goodenough, J. B.; Ikuta, H. Correlation between the Structure and the Spin State in $R_{1-x}Sr_xCoO_3$ (R=La, Pr, and Nd). *Phys. Rev. B*. **2007**, *76*, 144116.

(31) Jørgensen, J. E.; Keller, L. Magnetic Ordering in $HoBaCo_2O_{5.5}$. *Phys. Rev. B*. **2008**, *77*, 024427.

(32) Kazak, N. V.; Ivanova, N. B.; Michel, C. R.; Ovchinnikov, S. G.; Pashkevich, Y. G.; Balaev, A. D.; Bondarenko, G. V. Magnetic and Transport Properties of $Gd_{0.9}A_{0.1}CoO_{3-\delta}$ (A=Ba, Sr). *J. Magn. Magn. Mater.* **2009**, *321*, 1266-1271.

(33) Aksenova, T. V.; Gavrilova, L. Y.; Yaremchenko, A. A.; Cherepanov, V. A.; Kharton, V. V. Oxygen Nonstoichiometry, Thermal Expansion and High-Temperature Electrical

Properties of Layered $NdBaCo_2O_{5+\delta}$ and $SmBaCo_2O_{5+\delta}$. *Mater. Res. Bull.* **2010**, *45*, 1288-1292.
(34) Wang, Y.; Sui, Y.; Wang, X.; Su, W.; Cao, W.; Liu, X. Thermoelectric Response Driven by Spin-State Transition in $La_{1-x}Ce_xCoO_3$ Perovskites. *ACS Appl. Mater. Interfaces*. **2010**, *2*, 2213-2217.
(35) Matsumoto, Y.; Yamada, S.; Nishida, T.; Sato, E. Oxygen Evolution on $La_{1-x}Sr_xFe_{1-y}Co_yO_3$ Series Oxides. *J. Electrochem. Soc.* **1980**, *127*, 2360-2364.
(36) Jain, A. N.; Tiwari, S. K.; Singh, R. N.; Chartier, P. Low-temperature Synthesis of Perovskite-type Oxides of Lanthanum and Cobalt and Their Electrocatalytic Properties for Oxygen Evolution in Alkaline Solutions. *J. Chem. Soc., Faraday Trans. 1*. **1995**, *91*, 1871-1875.
(37) Bockris, J. O. M. The Electrocatalysis of Oxygen Evolution on Perovskites. *J. Electrochem. Soc.* **1984**, *131*, 290-302.
(38) Hastie, T.; Tibshirani, R.; Friedman, J., *The Elements of Statistical Learning*. Springer-Verlag: 2009.
(39) Child, D., *The Essentials of Factor Analysis*. 3rd ed.; Bloomsbury Academic: 2006.
(40) R Core Team *R: A Language and Environment for Statistical Computing*, R Foundation for Statistical Computing: Vienna, Austria, 2014.
(41) Benjamini, Y.; Hochberg, Y. Controlling the False Discovery Rate: A Practical and Powerful Approach to Multiple Testing. *J. Roy. Statist. Soc. Ser. B*. **1995**, *57*, 289-300.